HHS Public Access

Author manuscript

Neuroimage. Author manuscript; available in PMC 2020 October 01.

Published in final edited form as:

Neuroimage. 2019 October 01; 199: 153–159. doi:10.1016/j.neuroimage.2019.05.073.

In vivo serial MRI of age-dependent neural progenitor cell migration in the rat brain

Dorela D. Shuboni-Mulligan[1], **Shatadru Chakravarty**[1,2], **Christiane L. Mallett**[1,2], **Alexander Wolf**[1], **Pauline Dmitriev**[3], **Stacey Forton**[1], **Erik M. Shapiro**[1,2]

[1]Department of Radiology, Michigan State University, East Lansing, MI

[2]Institute for Quantitative Health Science and Engineering, Michigan State University, East Lansing, MI

[3]School of Medicine, Duke University, Durham, NC

Abstract

The subventricular zone (SVZ) is a neurogenic niche in the mammalian brain, giving rise to migratory neural progenitor cells (NPC). In rodents, it is well-established that neurogenesis decreases with aging. MRI-based cell tracking has been used to measure various aspects of neurogenesis and NPC migration in rodents, yet it has not yet been validated in the context of age-related decrease in neurogenesis. This validation is critical to using these MRI techniques to study changes in neurogenesis that arise in diseases prevalent in aging populations and their combination with advanced cellular therapeutic approaches aiming to combat neurodegeneration. As such, in this work we used MRI-based cell tracking to measure endogenous neurogenesis and cell migration from the SVZ along the rostral migratory stream to the olfactory bulb, for 12 days duration, in rats aged 9 weeks to 2 years old. To enable the specific detection of NPCs by MRI, we injected micron sized particles of iron oxide (MPIOs) into the lateral ventricle to endogenously label cells within the SVZ, which then appeared as hypo-intensive spots within MR images. *In vivo* MRI data showed that the rate of NPC migration was significantly different between all ages examined, with decreases in the distance traveled and migration rate as age progressed. The total number of MPIO-labeled cells within the olfactory bulb on day 12, was significantly decreased when compared across ages in *ex vivo* high-resolution scans. We also demonstrate for the first-time, provocative preliminary data suggesting age-dependent MPIO uptake within the dentate gyrus (DG) as well. Histology to identify doublecortin-positive NPCs, verified the decrease in cell labeling as a function of aging, for both regions. The dramatic reduction of NPC labeling within the SVZ observed with MRI, validates the sensitivity of MRI-based cell tracking to neurogenic potential and demonstrates the importance of understanding the impact of age on the relationship of NPC and disease.

Corresponding author: Erik M. Shapiro, Ph.D., Department of Radiology, Michigan State University, Radiology Building, 846 Service Road, East Lansing, MI 48824. shapir86@msu.edu.

6. CONFLICTS OF INTEREST

The authors declare no conflict of interest.

Graphical Abstract

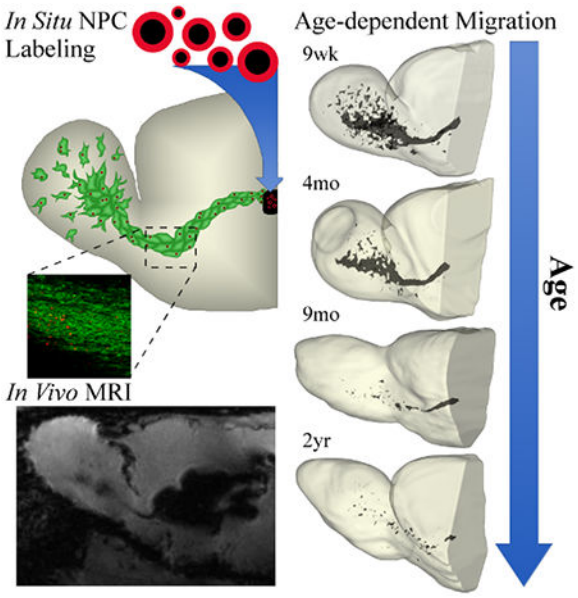

Keywords

Aging; Rostral Migratory Stream; Stem Cells; Iron Oxide; Cell Tracking

1. INTRODUCTION

Neurogenesis within the adult rodent brain primarily occurs in two regions: the subventricular zone (SVZ) of the lateral ventricle and the subgranular zone (SGZ) of the hippocampus (Altman, 1969; Kaplan & Hinds, 1977; Kaplan & Bell, 1984). Neural stem cells within the SVZ give rise to neural progenitor cells (NPC) which migrate from the lateral ventricle to the olfactory bulb (OB) via the rostral migratory stream (RMS) (Lois & Alvarez-Buylla, 1994; Lois et al., 1996). NPCs which migrate from the SGZ travel a much shorter distance into the dentate gyrus (DG, Rickmann et al., 1987; Seki et al., 2007). The migration rate of NPCs within these regions is dependent on environmental and physiological conditions, with aging greatly impacting neurogenesis within both regions. As animals age, the total number of proliferative cells decreases in both the SVZ (Apostolopoulou et al., 2017; Enwere et al., 2004) and SGZ (Kuhn et al., 1996). These cellular alterations in the substructure of the neurogenic regions have downstream effects that can observed within the RMS (Capilla-Gonzalez et al., 2013), OB (Enwere et al., 2004; Tropepe et al., 1997), and DG (Jin et al., 2003).

Quantifying NPC migration within the brain of aged animals has primarily been achieved using histological techniques; however, there is a growing literature using different imaging modalities to serially monitor endogenous NPC *in vivo* in live animals (Velde et al., 2012; Mallett, Shuboni-Mulligan & Shapiro, 2019). *In vivo* MRI paired with intraventricular injections of micron sized iron oxide particles (MPIOs) enables high resolution serial *in vivo* monitoring of endogenous NPC migration (Shapiro et al., 2006). NPCs labeled *in situ* have

been shown to progressively accumulate within the OB, with levels of cells depending on the location of injection and volume of MPIOs (Vreys et al., 2010; Granot et al., 2011). The optimal technique labels approximately 30% of NPCs within the RMS (Sumner et al., 2009) and within the OB, MPIOs were found primarily in immature neurons (Nieman et al., 2010;). The technique has been applied to both rat (Shapiro et al., 2006; Sumner et al., 2009; Granot et al., 2011) and mouse (Nieman et al., 2010; Vreys et al., 2010) but no direct species comparisons have been made with only some data suggesting species-specific variations in labeling at the SVZ (Nieman et al., 2010). MRI has been used to monitor ectopic migration of these cells in animal models of several disease states, including ischemia (Yang et al., 2008; Granot & Shapiro, 2014; Zhang et al., 2016). The presence of these cells in ischemic regions is hypothesized to improve neurological outcomes by promoting angiogenesis and by functioning as neuroprotective agents (Marlier et al., 2015). However, stroke and other diseases that recruit NPCs are more prevalent in older individuals (Wang et al., 2013) and the neurogenic response of these cells to disease is related to the age of animals (Gao et al., 2009). To make crucial translational experiments possible, it is critical to determine whether MRI-based cell tracking of endogenous neurogenesis accurately measures and is sensitive to age-related decrease in neurogenesis.

Previous histological studies have demonstrated a static snapshot of the progressive decrease in NPC migration away from the SVZ and SGZ. In this study we utilize our well-established technique of endogenously labeling NPCs within the SVZ with MPIOs and use MRI-based cell tracking to measure NPC migration into the OB as a function of age. We additionally use *in vivo* MRI to demonstrate that in older rats, NPCs have slower migration rates from the SVZ to the OB across 12 days and lower total amounts of NPC infiltration within the OB. We also, demonstrate provocative preliminary data suggesting age-dependent MPIO uptake within the DG as well. These results collectively demonstrate the importance of age-based differences of NPC within the SVZ and DG and highlight the benefit of within subject serial MRI as a tool for investigating migratory behavior.

2. METHODS

2.1 Animal Procedures

Rats were maintained under standard housing conditions in a 12:12 light/dark cycle with food and water *ad libitium*. All procedures were approved by the Institutional Animal Care and Use Committee at Michigan State University and are in accordance with the National Institutes of Health Guide for the Care and Use of Laboratory Animals (NIH Publications No. 8023, revised 1978).

Fischer 344 rats (Charles River, Raleigh, NC) were used in this study. Rats were separated into groups based on age: 9 weeks old (n=6), 4 months old (n=5), 9 months old (n=6), and 2 years old (n=4), and each underwent stereotactic surgery to inject MPIOs into the lateral ventricle. Intraventricular injections endogenously label NPCs within the SVZ, which can then be monitored longitudinally as cells migrate along the RMS into the OB using MRI (Shapiro et al, 2006). Serial MRI scans monitored the migration of NPCs over the course of 12 days, after which rats were sacrificed via transcardial perfusion. Brains were then

scanned *ex vivo* using a high-field 9.4T magnet at 50 μm resolution and then processed for histology using immunofluorescence.

2.2 Intraventricular Injection of MPIO for *In Situ* NPC Labeling

Prior to imaging, all rats were given intraventricular injections of Flash Red Fluorescent 1.63 μm MPIOs (ME04F, Bangs Laboratories, Fishers, IN; Fluorescence excitation and emission 660:690 nm) as previously described (Shapiro et al., 2006; Granot et al., 2011). In brief, rats were anesthetized with 2.5% isoflurane via endotracheal intubation using a 14G 2" catheter (ETT-16-50, Braintree Scientific, Inc., MA). Rats then were secured into a stereotaxic apparatus and a 3mm burr hole was drilled into the skull. A 50μL pressure injection was made using a Hamilton syringe with a 33G needle at AP: 0.3 mm, ML: 1 mm, DV:−3.5 mm (Figure S1). The needle was allowed to rest for 10 min and then slowly removed over the span of an additional 10 min. The skull was closed with bone wax and sutured, then rats were immediately scanned with an MRI.

2.3 *In vivo* MRI

Each rat underwent MRI 5 times over the course of 12 days: on day 0, immediately after injection, and then on days 1, 3, 6 and 12 post-injection. Prior to MRI, rats were intubated to anesthetize animals with isoflurane (2.5%) and secured onto the animal bed via ear and tooth bars. A 2×2 rat brain receive coil with volume coil transmission (Bruker Corporation, MA) was placed onto the head and rats were scanned with a 7T Bruker Biospec 70/30 USR using a FLASH sequence with the following parameters: TE = 10.44 ms, TR = 31 ms, FOV= 2.56 × 2.56 × 2 cm, resolution = 100 × 100 × 100 μm, averages = 2 and a total scan time = 47 min. Body temperature and breathing were continuously monitored (Model 1025; SA Instruments, Inc, NY). Rats were then given 1 mL of warmed saline after the 47 min scan and allowed to fully recover before being returned to their home cage.

2.4 *Ex vivo* MRI

After the final *in vivo* scan, rats were transcardially perfused with a 4% paraformaldehyde (PFA) solution doped with 1 mM Gd-DTPA (Magnevist, Bayer, NJ). Brains were extracted with care to preserve the OBs and post-fixed for at least 24hr in the Gd-DTPA-doped PFA. Brains were then placed into a 15mL Falcon tube filled with PBS. Tubes were fit into a volume coil and scanned on a 9.4T Bruker AVANCE at high resolution using a FLASH sequence with the following parameters: TE = 10 ms, TR = 30 ms, FOV = 2.56 × 1.92 × 1.92 cm, resolution = 50 × 50 × 50 μm, Averages = 10 and a total scan time= 12 hr 17 min.

2.5 Image Analysis

The images acquired during the *in vivo* scans were analyzed with the FIJI Measure tool (Schindelin et al., 2012) to determine the distance travelled by the particles from the SVZ to the olfactory bulb over time. The total volume of the particle distribution within the RMS and olfactory bulbs were measured with the *ex vivo* scans using the FIJI Analyze Particle tool after Thresholding. 3D Slicer 4.8 (Fedorov et al., 2012) was then used to create a 3D volume rendering of the RMS for a representative rat in each age group.

2.6 Immunofluorescence Histology

Brains were soaked for at least 24hr in 30% sucrose after the completion of imaging, then embedded in OCT and cut using a cryostat (Leica, Frankfurt, Germany) into 30μm sagittal sections. Free floating sections were stained for doublecortin (DCX). First, sections were blocked in 2% normal goat serum for 1hr and then incubated for 24hr at 1:2,000 of the primary antibody, rabbit anti-DCX (ab18723, Abcam). Sections were washed three times in PBS (10 min/wash) and then transferred into the 1:500 secondary antibody solution, goat anti-rabbit (ab150077, Abcam), for 1hr. Sections were mounted onto gelatinized slides, allowed to dry for 10 min and immediately coverslipped with ProLong Diamond Antifade Mountant (P36961, Life Technologies). Slides were allowed to cure at room temperature overnight and then stored at −20°C until microscopy.

Gross images of the RMS were acquired at 10× magnification for all samples using a Leica DMI4000B inverted fluorescence microscope. These images were used to determine the thickness of the RMS at the medial bend of the stream (Corona et al., 2016) with the FIJI software and the Measure tool. Images were additionally acquired at a higher magnification (20×) using a Nikon A1 Rsi confocal laser scanning microscope at three locations along the RMS: (1) posterior near the SVZ, (2) medial bend, and (3) anterior near the olfactory bulb.

2.7 Statistical Analysis

The statistical software SPSS (IBM, Armonk, NY) was used for all analysis. One-way ANOVAs were used to compare age groups. Groups were compared to one another for significant ANOVAs using independent samples t-test. Significance was defined as $p<0.05$.

3. RESULTS

3.1 MRI captures the impact of age on the rate of *in vivo* NPC migration

Many histological studies have observed the impact of age on the presence of NPC within the RMS, examining the number cells and size of the structure. Here, for the first time, we use MRI to examine the *in vivo* effects of age on NPC movement from the SVZ to the OB across 12 days (Figure 1). MPIOs injected into the rostral horn of the lateral ventricle can be observed immediately post injection (1 hr) as a dark blooming artifact within the structure. Within 24 hrs, MPIOs are taken up by neural stem cells within the SVZ and can be observed beginning their journey along the RMS in the 9 wk, 4 mo, and 9 mo rats, migrating anterior-ventrally from the SVZ and then arcing anterior-dorsally toward the OB. No migration is observed in 2 year old rats until day 12. Younger rats (9 wk and 4 mo) have NPCs that reach the OB by the third day, with maximal migration observed in the 9 wk cohort on day 12.

Quantification of the *in vivo* imaging data revealed that there were significant main effects of age ($F(3,15)= 43.1$, $p<0.001$) and time ($F(1,15)= 289.9$, $p<0.001$), but more importantly an interaction between age and time ($F(3,15)= 25.9$, $p<0.001$) (Figure 2). Generally, all age groups showed migration, however, there were different migration patterns over time between the age groups. To examine the difference in patterns, we fitted the 9 wk, 4 mo and 9 mo groups to linear, mono-exponential and bi-exponential curves (Figure S2). The least square means method showed higher R^2 values for the exponential fits in the 9 wk and 4 mo

groups when compared to the linear fitting. This allowed us to calculate half-lives of NPC migration from the SVZ to the OB for each cohort of rats: 2.6 days for the 9 wk cohort, 5.8 days for the 4 mo cohort and 17.4 days for the 9 mo cohort. Bi-exponential fits had higher R^2 values than the mono-exponential fits, suggesting changes in bulk migration rate during migration along the RMS for each cohort, yet corroborating this analysis requires further experimental confirmation, and is not part of this study. Exciting technologies for directly imaging cell migration at microscopic resolution, would be useful in deciphering this complex migration (Nam et al., 2007; Khlghatyan & Saghatelyan, 2012; Huang & Wang, 2019). In the 9 mo group, the R^2 were similar between all lines. Traditionally, this data has been calculated as NPC migration rate, which is the slope (μm/h) between each pair of time points, further demonstrating the exponential versus linear patterns observed between young (9 wk & 4 mo) and old (9 mo) groups, respectively (Table 1). Thus, MRI reveals that as rats age, for NPCs, the total distance traveled, and rate of migration decreases and importantly the pattern of migration is dramatically altered.

3.2 High Resolution imaging reveals the distribution of MPIO labeled cells within the OB across age

To measure the infiltration of migrating NPCs into the OB, we examined high resolution coronal MRI sections and quantified the percent labeling of migrating NPCs and compared these results between ages (Figure 3A–D). There was a significant effect of age in the total percentage of hypo-intensity seen within the interior of the OB ($F(3,17)= 11.145$, $p<0.001$). T-tests between the groups showed a significant difference between all ages for the number of cells migrating to the olfactory bulb (Figure 3E). When we examined the passive uptake of particles by quantifying the percentage of hypo-intensity on the outside of the OB, we found no significant difference between the groups ($F(3,17)= 1.031$, $p=0.409$; Figure 3F). This demonstrates that across all age groups the same amount of MPIOs are taken up by cells that line surfaces exposed to CSF which contain MPIOs, lending strength to the argument that the observed results are not due to differential initial labeling of NPCs at the SVZ.

To visualize the overall labeling of NPCs within rats, we generated 3D volume rendering for a representative rat in each age group (Figure 4). Visualizing the RMS in 2D slices does not provide a full view of all migrating cells; this was particularly evident in older rats who had fewer labeled cells. These 3D renderings demonstrate the total distribution of cells within the RMS and OB at day 12 across all slices and again showed the greatest labeling in the youngest rat and the least in the oldest.

3.3 Histological comparison of DCX-labeled cells within the RMS mirrors MRI findings

To verify the differences seen with MRI as a function of rat age, we additionally examined the histology of brain section using DCX labeling (Figure 5A), a marker associated with NPCs. Using fluorescence microscopy, we measured the width of the RMS at the medial bend, where the stream is widest. There was a significant difference in width between the age groups ($F(3,15)= 69.340$, $p<0.001$). T-tests between the groups showed a significant difference between all ages, with smaller lengths as rats aged (Figure 5B). Confocal

microscopy of three regions across the RMS demonstrated that at all levels of the structure, older rats had less DCX labeling for all regions photographed (Figure 6).

3.4 Novel identification of age-dependent MPIO labeling within the DG of the hippocampus

The DG of the hippocampus also has a population of NPCs, however this region has never been examined for labeling with MPIOs. Here we make a novel discovery of age-based variation in MPIO labeling within the DG. In our *in vivo* scans, blooming artifacts caused by the presence of MPIOs within the ventricle obscure the visibility of the hippocampus (Figure S3). After rat sacrifice and perfusion, the amount of MPIOs was reduced within the ventricles around the hippocampus, allowing for high resolution imaging of the region. *Ex vivo* scans within the caudal portion of the DG showed a marked uptake of particles within young rats and a decrease in uptake as rats aged (Figure 7A). Analysis of the percentage of MPIOs within the hippocampus showed a significant effect of age ($F(3,17)= 6.27$, $p=0.003$) (Figure 7B). The younger rats, 9 wk and 4 mo, had more MPIO than the 9 mo and 2 yr rats. Histological labeling of the rostral DG demonstrates that a younger rat has greater DCX labeling in the region than an older rat (Figure S4).

4. DISCUSSION

Labeling endogenous NPCs with iron oxide particles is a well-established technique for monitoring the *in vivo* migration of NPCs from the SVZ into the OB using MRI (Shapiro et al., 2006). In this study, we validate the use of *in vivo* MRI-based cell tracking to measure age-based differences in NPC migration from the SVZ to the OB *in vivo*, and verify these findings with high resolution *ex vivo* MRI and histology. We also highlight the possible use of the technique to observe NPC migration within another neurogenic region, the DG. Understanding the physiology and behavior of these self-renewing cells gives insight into how the brain responds and recovers from stressors, such as injury and disease.

As rodents age, there is a clear impact on the neurogenic population of cells found in the SVZ. Histological studies have established that there are significant changes in the structure of the region, with a reduction in the total number of proliferative cells. Specifically, by middle-age (12 months) rats have a significant reduction in the expression of Sox2 and DCX (Bouab et al., 2011) and by old age (> 22 months) the cells are almost completely depleted (Capilla-Gonzalez et al., 2013). These decreases in neural stem cells within the SVZ lead to a dramatic change in the appearance of the RMS, as 2 year old rats have almost no DCX-stained (Capilla-Gonzalez et al., 2013) or Brd-U-stained (Mobley et al., 2013) migrating NPCs when compared to young controls. With histology, we observed similar decreases across ages in DCX-positive NPCs in the RMS. Younger 9 week and 4 month old rats had high numbers of DCX-positive NPCs in the RMS while older 9 month and 2 year old rats had lower numbers with a RMS that appeared significantly thinned (Figure 6). Our study further showed that age-related decrease in DCX-positive NPCs in the RMS typically observed in histology, are similar to those observed on MRI.

Our results demonstrated that age directly impacts the rate at which NPCs migrate into the olfactory bulb (Figure 1 & 2). *In vivo* imaging by labeling NPCs with MPIOs and

performing serial, *in vivo* MRI allows for continued monitoring of NPC across time and within subjects. Using this technique, NPC migration rates in young mouse and rats (6-10 weeks) has been established as 102-120μm/h on day 0-1 (Nieman et al., 2010; Pothayee et al., 2017) which decreases to 49 μm/h on day 2 (Nieman et al., 2010). These results are similar to the NPC migration rates measured for 9 week old rats in this manuscript (Table 1) and also identical to NPC migration rates measured in histological studies using organotypic brain slices (Hirota et al., 2007; Kaneko et al., 2010) and in cell culture. Our data further shows that as NPCs migrate closer to the OB, the bulk migration rate exponentially decreases. This could be due to cells changing their migration rates during the journey from the RMS to the OB, or that there are a populations of cells that migrate faster than others. Both phenomena have been observed for NPCs in the rodent RMS using live cell microscopy (Nam et al., 2007; Khlghatyan & Saghatelyan, 2012) . Cells migrate along the RMS in a chain through an astrocytic tunnel (Lois, Garcia-Vardugo & Alvarez-Buylla, 1996) but alter their migration pattern, moving radially rather than tangentially, once they reach the OB (Saghatelyan et al., 2004). The difference between the two environments, both structurally and molecularly (for review; Kaneko, Sawada & Sawamoto, 2017), may lead to the altered rates of migration observed within the RMS and the radial migration in the OB. It is important to note that we observed no size differences in the whole brain or relative OB size across our ages (Figure S5) which is identical to previous publications (Casas et al., 2018; Hamezah et al. 2017).

In older rats, our data also shows a stark decrease in the migration rate as the rats age. Mobley *et al.* (2013) demonstrated that at 14 days post-BrdU injection, the number of migrated NPCs decrease as rats age at the three points along the RMS (the posterior near the SVZ, the medial bend, and the anterior near the olfactory bulb). Many studies have highlighted the importance of NPC depletion across age (Apostolopoulou et al., 2017; Enwere et al., 2004) but clearly, our findings support the notion that either the RMS architecture that enables migration, or NPC migration ability, or both, are directly impacted by age as migration rates are greatly decreased in older rats (Capilla-Gonzalez et al., 2013). Alternatively, previous studies have demonstrated developmental stage dependent presence of chemorepellents (i.e. Slit2) and their receptors (i.e. Robo1) which may also alter the rate of migration (Guerrero-Cazares et al., 2017). These findings further bring into question the validity of using young animals for regenerative medicine studies, if the target disease population is aged with different NPC levels and migratory capabilities, unless it can be shown that with injury, neurogenesis is increased to levels equivalent to young animals.

The DG of the hippocampus is another neurogenic population of cells negatively impacted by the aging process (Ben Abdallah et al., 2010), with steady decreases in the number of Nestin-positive cells, a marker for NPCs, observed as mice age from 3 weeks to 24 months (Encinas et al., 2011). In our *ex vivo* scans, we observed clear differences in the number and distribution of labeled cells within the DG (Figure 5). In the 9 week old rats, there are many hypointense dark spots, generally associated with labeled cells distributed widely across the caudal portion of the hippocampus. The number of spots decreases in a similar fashion as the histological studies across age. Our histology also demonstrates a decrease in the amount of DCX staining observed within the region between the youngest and oldest rats. However,

in depth analysis is required to verify which cell types uptake particles and to quantify the degree of labeling.

5. CONCLUSION

Dynamic changes in NPC migration as a function of animal age is a critical variable for developing effective treatment for regenerative medicine because neurodegenerative disorders are more prevalent in older individuals. Herein, we apply MRI-based cell tracking to monitor NPC migration *in vivo* to non-invasively study age-based neurogenesis. We verified that the MRI technique matches histological findings between young and old groups, demonstrating that few NPC are found in the RMS and OB as rats age. Further, we, for the first time, quantified the rate of migration over 12 days across all age groups and determined *ex vivo* that particles integrate into the caudal portion of the DG.

Supplementary Material

Refer to Web version on PubMed Central for supplementary material.

ACKNOWLEDGMENTS

The authors are grateful for the assistance provided by the MSU Center for Advanced Microscopy, specifically to Dr. Melinda Frame for her technical support. We also thank the members of the MSU MCIL for providing critical feedback of the work. This work was supported by grants from the National Institutes of Health (R01 DK107697 to EMS).

Abbreviations:

MPIOs	micron sized particles of iron oxide
SVZ	subventricular zone
NPC	neural progenitor cells
SGZ	subgranular zone
OB	olfactory bulb
RMS	rostral migratory stream
DG	dentate gyrus
PFA	paraformaldehyde
DCX	doublecortin

References:

Altman J (1969) autoradiographic and histological studies of postnatal neurogenesis. IV. Cell proliferation and migration in the anterior forebrain, with special reference to persisting neurogenesis in the olfactory bulb. J Comp Neurol, 137(4):433–457. [PubMed: 5361244]

Apostolopoulou M, Kiehl TR, Winter M, de la Hoz EC, Boles NC, Bjorsson CS, Zuloaga KL, Goderie SK, Wang Y, Cohen AR, and Temple S (2017) Non-montonic changes in progenitor cell behavior

and gene expression during aging of the adult V-SVZ neural stem cell niche. Stem Cell Reports, 9:1931–1947. [PubMed: 29129683]

Ben Abdallah NM, Slomianka L, Vyssotski AL, Lipp HP (2010) Early age-related changes in adult hippocampal neurogenesis in C57 mice. Neurobiol Aging 31(1): 151–161. [PubMed: 18455269]

Bouab M, Paliouras GN, Aumont A, Forest-Berard K, and Fernandes KJ (2011) Aging of the subventricular zone neural stem cell niche: evidence for quiescence-associated changes between early and mid-adulthood. Neuroscience, 173: 135–149. [PubMed: 21094223]

Capilla-Gonalez V, Cebrian-Silla A, Guerrero-Cazares H, Garcia-Verdugo JM, and Quinones-Hinojosa A (2013) The generation of Oligodendroglial cells is preserved in the rostral migratory stream during aging. Front Cell Neurosci, 7:147. [PubMed: 24062640]

Casas R, Muthusamy S, Wakim PG, Sinharay S, Lentz MR, Reid WC, & Hammoud DA (2018). MR brain volumetric measurements are predictive of neurobehavioral impairment in the HIV-1 transgenic rat. NeuroImage: Clinical, 17, 659–666. [PubMed: 29204344]

Corona R, Retana-Marquez S, Portillo W, and Paredes RG (2016) Sexual behavior increases cell proliferation in the rostral migratory stream and promotes the differentiation of the new cells into neurons in the accessory olfactory bulb of female rats. Front. Neurosci,10:48. [PubMed: 26955325]

Encinas JM, Michurina TV, Penunova N, Park JH, Tordo J, Peterson DA, Fishell G, Koulakov A, and Enikolopov G (2011) Division-coupled astrocytic differentiation and age-related depletion of neural stem cells in the adult hippocampus. Cell Stem Cell, 8(5):566–579. [PubMed: 21549330]

Enwere E, Shingo T, Gregg C, Fujikawa H, Ohta S, and Weiss S (2004) Aging results in reduced epidermal growth factor receptor signaling, diminished olfactory neurogenesis, deficits in fine olfactory discrimination. The Journal of Neuroscience, 24(38):8354–8365. [PubMed: 15385618]

Fedorov A, Beichel R, Kalpathy-Cramer J, Finet J, Fillion-Robin J-C, Pujol S, Bauer C, Jennings D, Fennessy FM, Sonka M, Buatti J, Aylward SR, Miller JV, Pieper S, and Kikinis R (2012) 3D Slicer as an Image Computing Platform for the Quantitative Imaging Network. Magn Reson Imaging, 30(9):1323–41. [PubMed: 22770690]

Gao P, Shen F, Gabriel RA, Law D, Yang E, Yang GY, Young WL, and Su H (2009) Attenuation of brain response to VEFG-mediated angiogenesis and neurogenesis in aged mice. Stroke 40(11): 3596–3600. [PubMed: 19745179]

Granot D, Scheinost D, Markakis EA, Papademetris X, and Shapiro EM (2011) Serial monitoring of endogenous neuroblast migration by cellular MRI. Neuromage, 57:817–824.

Granot D and Shapiro EM (2014) Accumulation of Micron Sized Iron Oxide Particles in Endothelin-1 Induced Focal Cortical Ischemia in rats is independent of cell migration. Magnetic Resonance in Medicine, 71: 1568–1574. [PubMed: 23661604]

Hamezah HS, Durani LW, Ibrahim NF, Yanagisawa D, Kato T, Shiino A, Tanaka S, Damanhuri HA, Ngah WZW, & Tooyama I (2017). Volumetric changes in the aging rat brain and its impact on cognitive and locomotor functions. Experimental gerontology, 99, 69–79. [PubMed: 28918364]

Hirota Y, Ohshima T, Kaneko N, Ikeda M, Iwasato T, Kulkarni AB, Mikoshiba K, Okano H, and Sawamoto K (2007) Cyclin-dependent kinase 5 is required for control of neuroblast migration in the postnatal subventricular zone. The Journal of Neuroscience, 27(47):12829–12838. [PubMed: 18032654]

Huang Z, & Wang Y (2019). In Vivo Electroporation and Time-Lapse Imaging of the Rostral Migratory Stream in Developing Rodent Brain. Current protocols in neuroscience, e65. [PubMed: 30861320]

Jin K, Sun Y, Xie L, Batteur S, Mao XO, Smelick C, Logvinova A, and Greenberg DA (2003) Neurogenesis and aging: FGF-2 and HB-EGF restore neurogenesis in hippocampus and subventricular zone of aged mice. Aging Cell, 2:175–183. [PubMed: 12882410]

Kaneko N, Marin O, Koike M, Hirota Y, Uchiyama Y, Wu JY, Lu Q, Tessier-Lavigne M, Alvarez-Buylla A, Okano H, Rubenstein JLR, and Sawamoto K (2010) New neurons clear the path of astrocytic processes for their rapid migration in the adult brain. Neuron, 67:213–223. [PubMed: 20670830]

Kaneko N, Sawada M, and Sawamoto K (2017) Mechanisms of neuronal migration in the adult brain. J Neurochem, 141(6):835–847. [PubMed: 28251650]

Kaplan MS and Bell DH (1984) Mitotic neuroblasts in the 9-day-old and 11-month-old rodent hippocampus. The Journal of Neuroscience, 4(6):1429–1441. [PubMed: 6726341]

Kaplan MS and Hinds JW (1977) Neurogenesis in the adult rat: electron microscopic analysis of light radioautographs. Science, 197(4308):1092–1094. [PubMed: 887941]

Khlghatyan J, & Saghatelyan A (2012). Time-lapse imaging of neuroblast migration in acute slices of the adult mouse forebrain. JoVE (Journal of Visualized Experiments), (67), e4061. [PubMed: 23007608]

Kuhn HG, Dickinson-Anson H, and Gage FH (1996) Neurogenesis in the dentate gyrus of the adult rat:age-related decrease of neuronal progenitor proliferation. The Journal of Neuroscience, 16(6): 2027–2033. [PubMed: 8604047]

Lois C, Garcia-Verdugo J, and Alvarez-Buylla A (1996) Chain migration of neuronal precursors. Science, 271(5251):978–981. [PubMed: 8584933]

Lois C and Alvarez-Buylla (1994) Long-distance neuronal migration in the adult mammalian brain. Science, 264(5162):1145–1148. [PubMed: 8178174]

Mallett C, Shuboni-Mulligan D, Shapiro E (2019) Tracking neural progenitor cell migration in the rodent brain using magnetic resonance imaging. Frontiers in Neuroscience, 12: 995. [PubMed: 30686969]

Marlier Q, Verteneuil S, Vandenbosch R, and Malgrange B (2015) Mechanisms and functional significance of stroke-induced neurogenesis. Frontiers in Neuroscience, 9:458. [PubMed: 26696816]

Mobley A, Bryant AK, Richard MB, Brann JH, Firestein SJ, and Greer CA (2014) Age-dependent regional changes in the rostral migratory stream. Neurobiol Aging, 34(7): 1873–1881.

Nam SC, Kim Y, Dryanovski D, Walker A, Goings G, Woolfrey K, Kang SS, Chu C, Erdelyi F, Szabo G, Hockberger P, & Szabo G (2007). Dynamic features of postnatal subventricular zone cell motility: A two-photon time-lapse study. Journal of Comparative Neurology, 505(2), 190–208. [PubMed: 17853439]

Nieman BJ, Shyu JY, Rodrigez JJ, Garcia AD, Joyner AL, and Turnbull DH (2010) In vivo MRI of neural cell migration dynamics in the mouse brain. NeuroImage 50:456–464. [PubMed: 20053381]

Pothayee N, Cummings DM, Schoenfeld TJ, Dodd S, Cameron HA, Belluscio L, and Koretsky AP (2017). Magnetic resonance imaging of odorant activity-dependent migration of neural precursor cells and olfactory bulb growth. NeuroImage, 158:232–241. [PubMed: 28669915]

Rickmann M, Amaral DG, and Cowan WM (1987) Organization of radial glial cells during the development of the rat dentate gyrus. J Comp Neurol, 264(4):449–479. [PubMed: 3680638]

Saghatelyan A, de Chevigny A, Schachner M, and Lledo PM (2004) Tenascin-R mediates activity-dependent recruitment of neuroblasts in the adult mouse forebrain. Nat Neurosci, 7(4):347–356. [PubMed: 15034584]

Schindelin J, Arganda-Carreras I, and Frise E et al. (2012) “Fiji: an open-source platform for biological-image analysis”, Nature methods 9(7): 676–682, doi:10.1038/nmeth.2019 [PubMed: 22743772]

Seki T, Namba T, Mochizuki H, and Onodera M (2007) Clustering, migration, and neurite formation of neural progenitor cells in the adult rat hippocampus. J Comp Neurol, 502:275–290. [PubMed: 17348003]

Shapiro EM, Gonzalez-Perez O, Garcia-Verdugo JM, Alvarez-Buylla A, and Koretsky AP (2006a) Magnetic resonance imaging of the migration of neuronal precursors generated in the adult rodent brain. NeuroImage 32:1150–1157. [PubMed: 16814567]

Sumner JP, Shapiro EM, Maric D, Conroy R, and Koretsky AP (2009) In vivo labeling of adult neural progenitors for MRI with micron sized particles of iron oxide: Quantification of labeled cell phenotype. NeuroImage 44:671–678. [PubMed: 18722534]

Tropepe V, Craig CG, Morshead CM, and van der Kooy D (1997) Transforming growth factor-α null and senescent mice show decreased neural progenitor cell proliferation in the forebrain subependyma. The Journal of Neuroscience, 17(20):7850–7859. [PubMed: 9315905]

Velde GV, Couillard-Despres S, Algner L, Himmelreich U, and van der Linden A (2012) In situ labeling and imaging of endogenous neural stem cell proliferation and migration. Wiley Interdiscip Rev Nanomed Nanobiotechnol, 4(6):663–679. [PubMed: 22933366]

Vreys R, Velde GV, Krylychkina O, Vellema M, Verhoye M, Timmermans JP, Baekelandt V, and Van der Linden A (2010) MRI visualization of endogenous neural progenitor cell migration along the RMS in the adult mouse brain: Validation of various MPIO lebeling strategies. NeuroImage, 49:2094–2103. [PubMed: 19850132]

Wang Y, Rudd AG, and Wolfe CDA (2013) Age and ethnic disparities in incidence of stroke over time: The South London Stroke Register. Stroke, 44:3298–3304. [PubMed: 24114452]

Yang J, Liu J, Niu G, Liu Y, & Wu EX (2008). Magnetic resonance imaging of migrating neuronal precursors in normal and hypoxic-ischemic neonatal rat brains by intraventricular MPIO labeling. In Engineering in Medicine and Biology Society, 2008. EMBS 2008. 30th Annual International Conference of the IEEE (pp. 363–366). IEEE.

Zhang F, Duan X, Lu L, Zhang X, Zhong X, Mao J, Chen M, and Shen J (2016) In vivo targeted MR imaging of endogenous neural stem cells in ischemic stroke. Molecules, 21:1143.

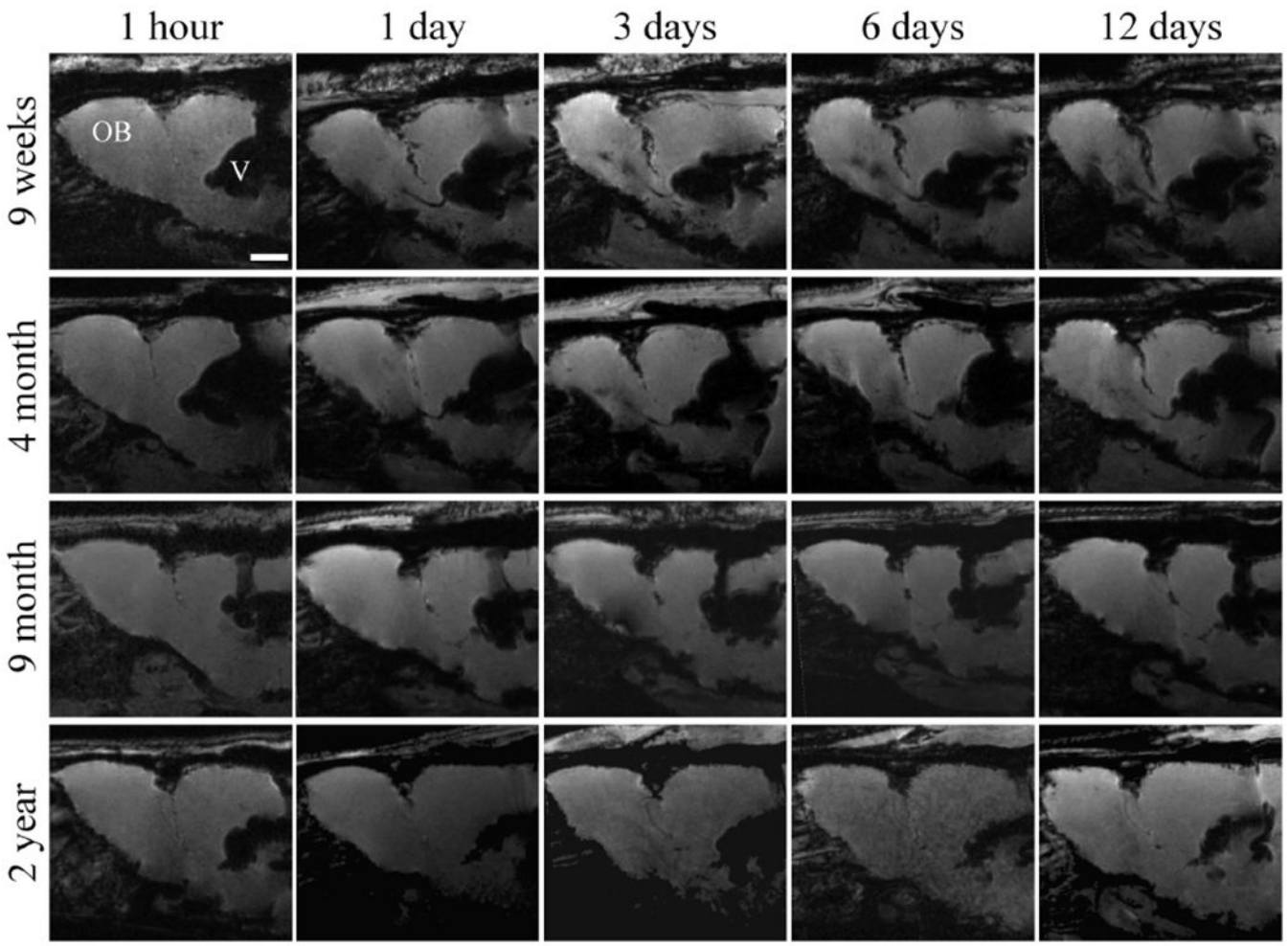

Figure 1.

In vivo 7T MR images of representative rats from each age group at five time points post-injection of MPIOs. The RMS (or lack thereof) can be observed extending from the lateral ventricle (V) into the olfactory bulb (OB). Scale bar in the top left image represent 2000 μm.

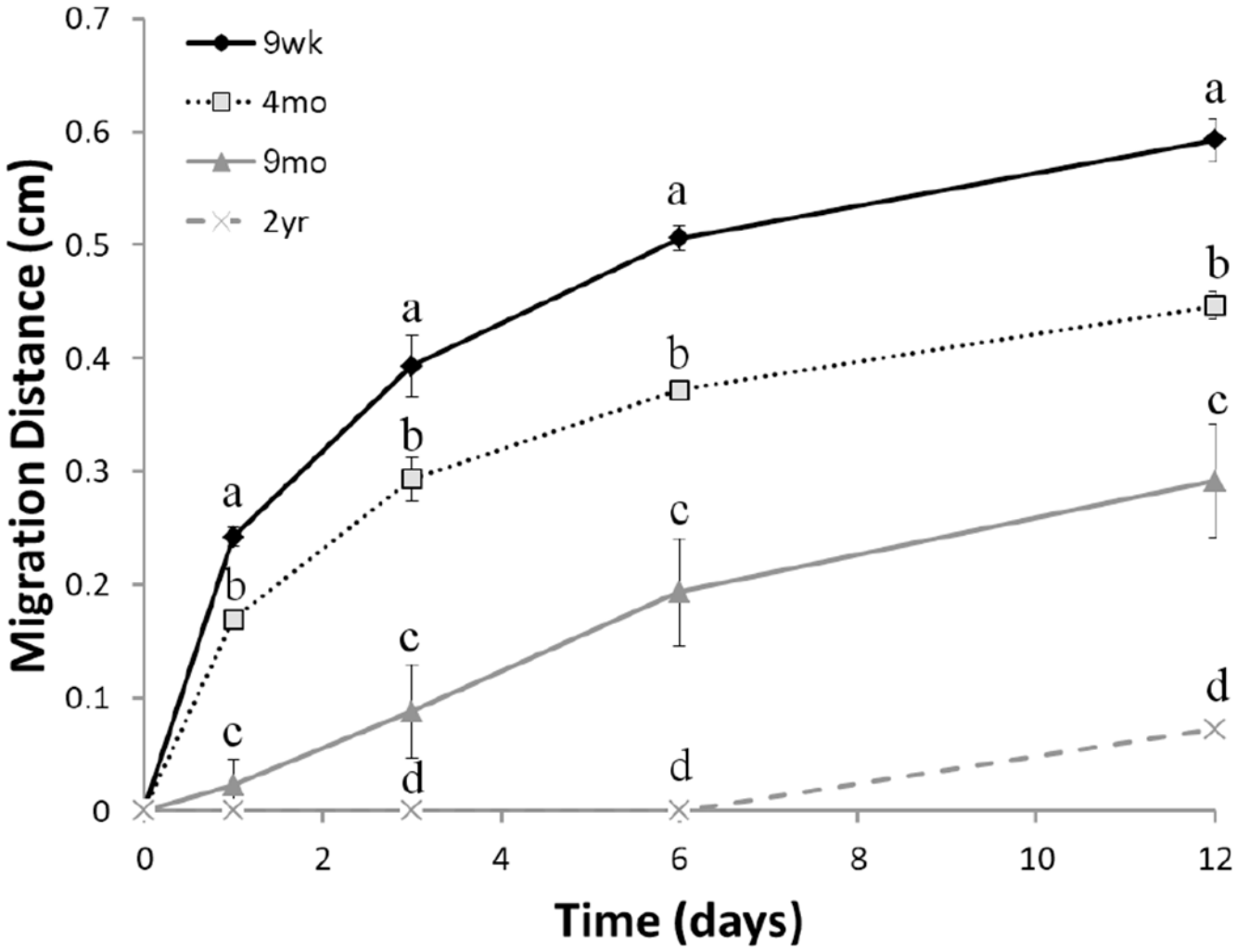

Figure 2.

Quantitative evaluation of migration distance for all rats in each age group across time. Points represent mean of each age group at each time point ±SEM. Different letters represent significance difference (p<0.05) between age groups at each time point.

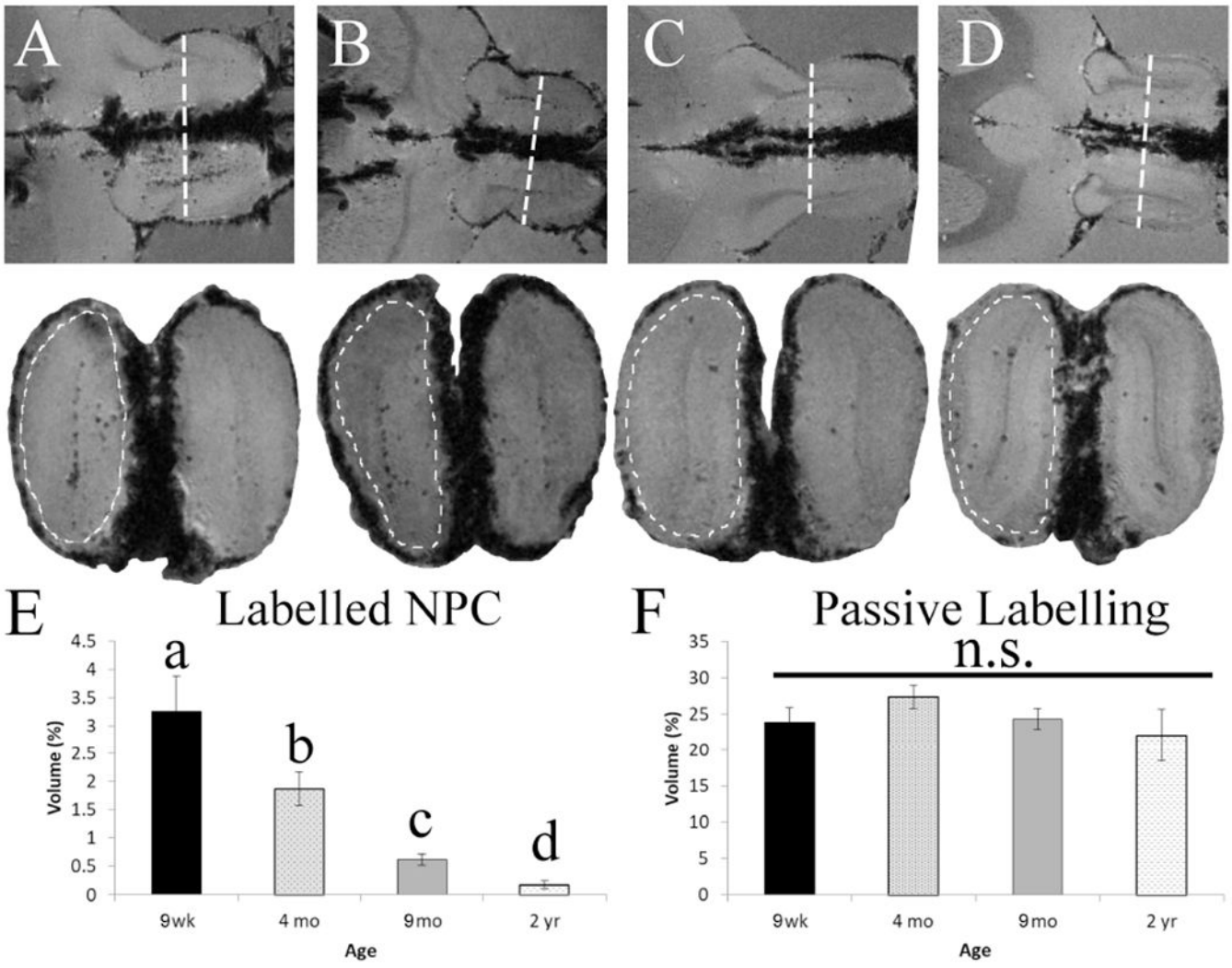

Figure 3.

Ex vivo MR images in horizontal and coronal planes and analysis of MPIO quantity within the olfactory bulb. (A-D) Demonstrate the horizontal view (upper panel) of the rostral migratory stream (RMS) with a line indicating the level of the coronal section (lower panel), the dotted line denotes the outer passive labeling region from the migrating cells internally. (E) Quantifies the percentage of hypointense area found in the internal portion of the coronal section at each age group. The different letters indicate groups that are significantly different from one another ($p<0.05$). (F) Quantifies the percentage of total hypointense area found outside of the internal labeling, which is cause by uptake of particles from the CSF by non-migrating cells.

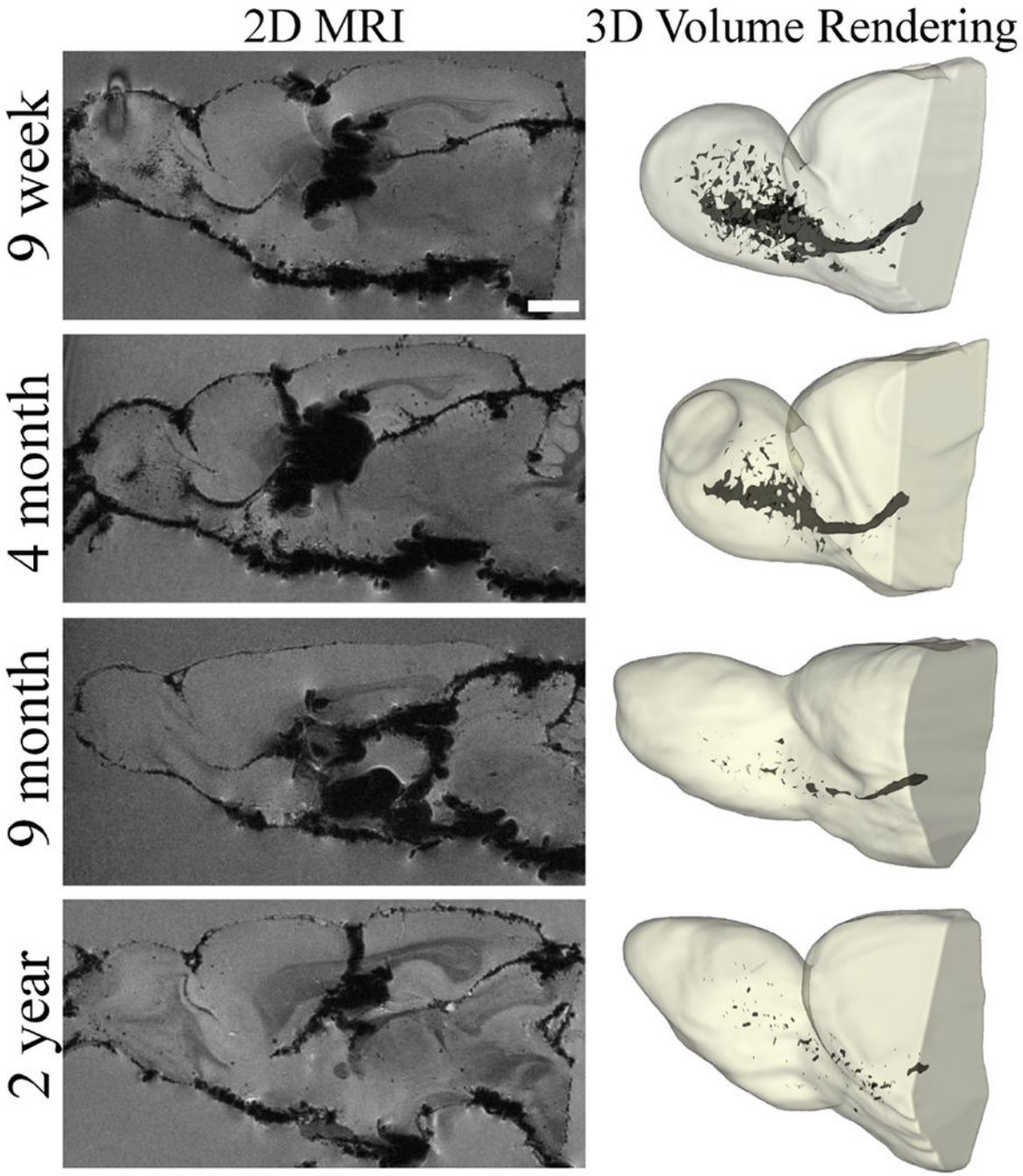

Figure 4.

Ex vivo 9.4T MR images of the RMS displayed in two and three dimensional format for all age groups. The left column has examples of the best representative slices of the RMS in 2D, while the right column is a 3D rendering of the same rat with all MPIO containing cells of the RMS highlighted in dark grey. Scale bar in the top left image represent 2000 μm for the 2D images.

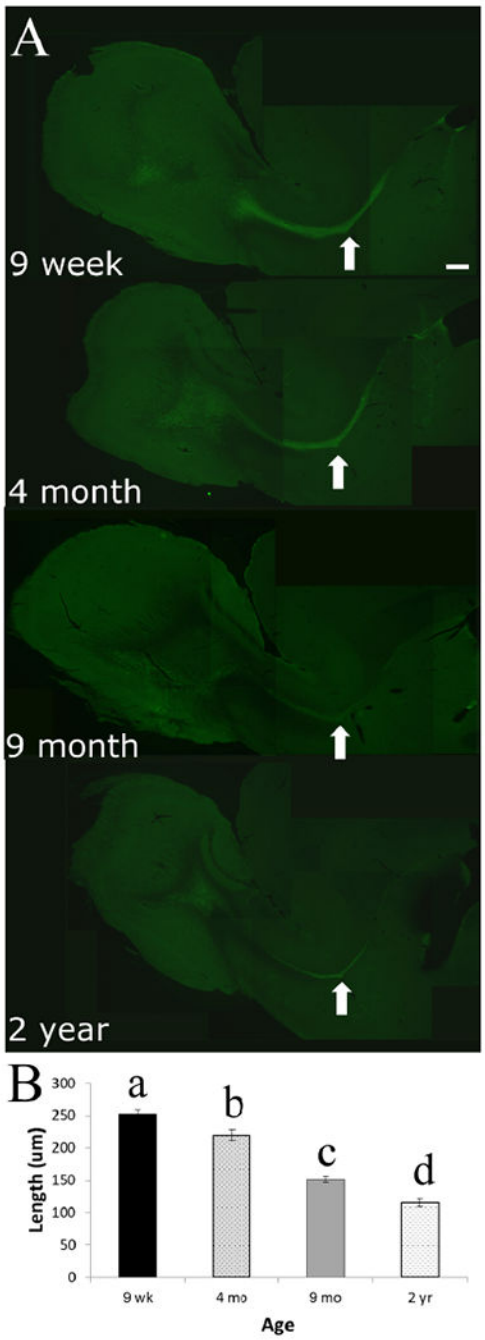

Figure 5.

Fluorescent microscopy images and analysis of DCX labeling within the brains of rats across all age groups. (A) Representative images for the four age groups, the arrow denotes the medial bend of the RMS where measurements of length were taken. The scale bar represents 500 μm. (B) Graphical representation depicting the mean ±SEM of thickness (length, μm) of the RMS at the medial bend for all age groups. Different letters denote significant difference between the groups ($p<0.05$).

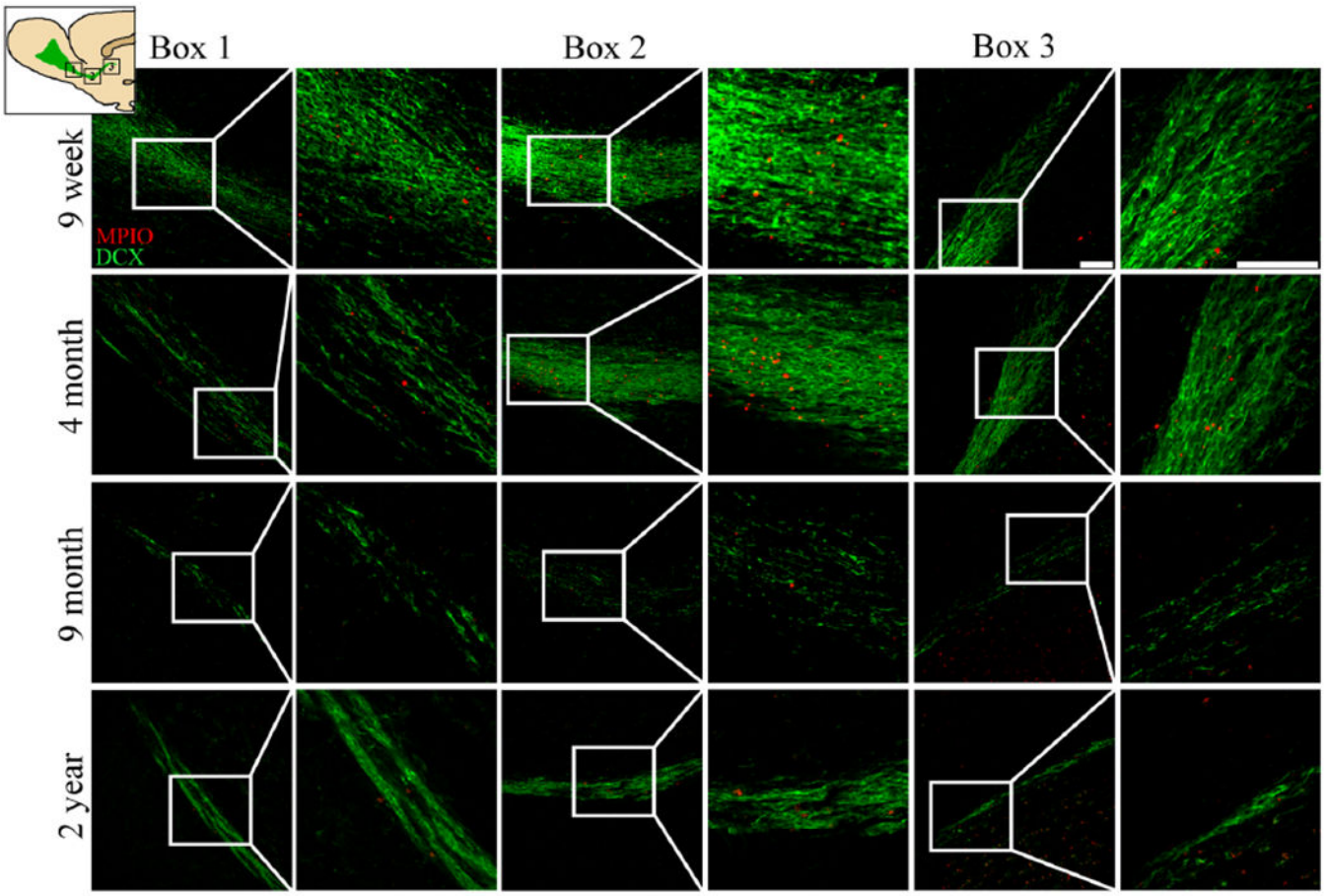

Figure 6.

Confocal microscopy images of three locations along the RMS for all age groups. The diagram in the upper left corner denotes the location of the images taken along the RMS: Box 1 is positioned anterior near the OB, Box 2 at the medial bend of the RMS, and Box 3 is posterior near the SVZ. A representative from each age was selected for each row. The green within each image is DCX staining and the red represent fluorescent MPIOs. The scale bar on the top right image is 100 μm.

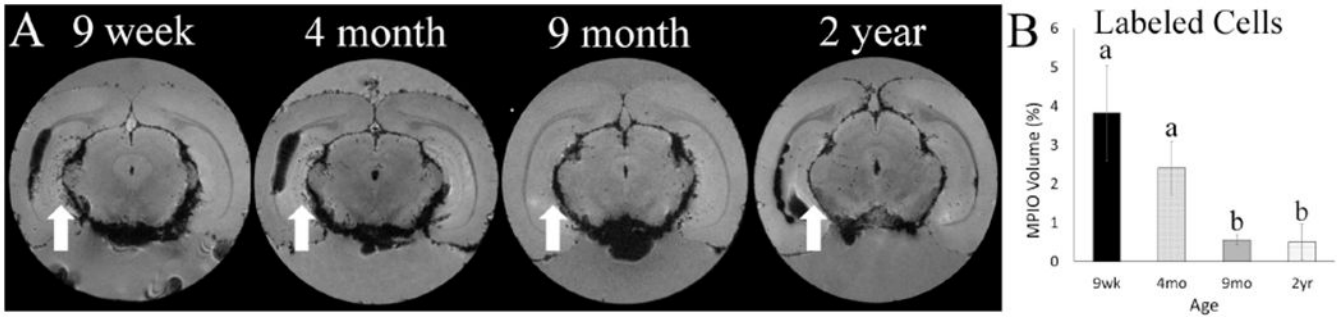

Figure 7.

MPIO labeling within the DG of the hypothalamus. (A) Representative 9.4T MR images acquired in *ex vivo* samples, dark hypotensive spots represent cells labeled with MPIOs. The white arrows denote the DG in rats at each age. (B) Quantification of MPIO labeling in the DG, different letters represent significance difference ($p<0.05$) between age groups.

Table 1.

Average Rate of NPC migration (μm/h) across age

	0-1d	1-3d	3-6d	6-12d
9 wk	100.8±3.4	31.5±4.4	15.7±3.4	6.0±1.8
4 mo	70.5±2.9	25.8±3.8	10.9±1.9	5.2±0.8
9 mo	9.4±9.4	13.6±6.5	14.7±4.0	6.8±1.0
2 yr	0	0	0	5.0±0.2

Note: Reported as mean ± SEM.